Nanoscale Morphology Control of Polymer/TiO_2 Nanocrystal Hybrids: Photophysics, Charge Generation, Charge Transport, and Photovoltaic Properties

Chia-Hao Chuang,[†] Yun-Yue Lin,[†] Yun-Heng Tseng, Tsung-Hung Chu, Chih-Cheng Lin, Wei-Fang Su, and Chun-Wei Chen*

Department of Materials Science and Engineering, National Taiwan University, Taipei 106, Taiwan

Received: August 10, 2010; Revised Manuscript Received: September 19, 2010

We present a simple approach by using mixed solvent to control the morphology of poly(3-hexylthiophene) (P3HT)/TiO_2 nanorod hybrid bulk heterojunction solar cells without any post-treatment. The effects of the controlled morphology on the optical and electrical properties are investigated. It has been a challenge to disperse polar inorganic nanocrystals at a relative high concentration into a relative nonpolar polymer. The use of mixed solvent which consists of pyridine (a poor solvent for P3HT), dichloromethane, and chloroform (a good solvent for P3HT) modifies the nanoscale morphology of P3HT/TiO_2 nanorod hybrids, resulting in highly crystalline P3HT domains with well-dispersed TiO_2 nanorods within polymer matrix. Study of photophysics reveals that charge carrier could form from emissive species upon photoexcitation and such a process is more efficient in highly ordered P3HT prepared by mixed solvent method. In the P3HT/TiO_2 hybrid film, the formation of a bicontinuous phase-separated morphology largely improves charge separation, transport, and recombination in the hybrid devices, which are further supported by time-resolved photoluminescence spectroscopy, carrier extraction by linearly increasing voltage mobility measurement, and transient open-circuit voltage decay measurement, respectively. A result of threefold improvement of the device performance using mixed solvent has been demonstrated compared to that using a single solvent only. This simple process does not need any further thermal post-treatment and is therefore compatible with the room temperature process developed with commonly used plastic substrates for flexible solar cell applications. Our method for morphology control could also be applied to other donor−acceptor hybrid systems as a strategy for device optimization.

1. Introduction

In the past decades, polymer solar cells have attracted a great of interest in developing low-cost, large-area, mechanically flexible photovoltaic devices.[1,2] The most common polymer photovoltaic device is based on bulk heterojunctions (BHJs), which consist of an electron-accepting network formed randomly within the polymer matrix. The nanoscale phase separation of BHJs creates efficient donor/acceptor interfaces for exciton dissociation and charge transfer. The formation of a bicontinious network can facilitate the free carriers of electrons and holes to transport toward electrodes to generate electricity. Extensive research has been focused on the development of polymer photovoltaic devices using fullerene or fullerene derivatives as acceptors, and a power conversion efficiency of over 6% has been reported.[3] Another promising type of acceptor in polymer solar cells is based on inorganic semiconductor nanocrystals, owing to the advantage of relatively high electron mobility and good physical and chemical stability.[4] Various types of inorganic nanocrystals such as TiO_2,[4−6] CdSe,[7,8] PbS,[9] and ZnO[10,11] have been used in polymer/inorganic hybrid BHJ solar cells. TiO_2 nanocrystals are one of the very promising candidates for BHJ solar cells since they are environmentally friendly and low-cost in fabrication. However, the reported efficiencies devoted to the polymer/TiO_2 nanocrystal hybrid BHJ solar cells are still low due to the strong incompatibility of the inorganic nanocrystals and polymer.[4] Until recently, we have demonstrated a promising power conversion of 2.2% of a polymer photovoltaic device based on poly(3-hexylthiophene) (P3HT)/TiO_2 nanorod BHJs through interface modification between P3HT and TiO_2 nanorods.[6] Removal of an insulating ligand or attachment of an effective interface modifier on TiO_2 nanorod surface can facilitate charge transfer and suppress charge recombination at P3HT/TiO_2 interfaces, leading to a significant improvement of the device performance.[6,12]

In solution processing, fast solvent evaporation rate makes self-organization and phase separation kinetically limited. Therefore, morphology control remains crucial for device design. Thermal annealing[13] and solvent annealing[14] are the common methods to improve the device performance. Recently, the use of mixed solvent or processing additives has been shown a successful method to improve the performance of polymer transistors[15] and polymer-based photovoltaic devices.[8,16−20] In our previous reports, P3HT/TiO_2 BHJ solar cells with relatively high power conversion efficiency were also fabricated by using mixed solvent.[6,12] It has been a challenge to disperse polar nanocrystals at a relative high concentration into a relative nonpolar polymer. The surface of as-synthesized nanocrystals is usually capped with surfactants, which contain long alkyl chains acting as a barrier for charge transport and charge transfer.[12] Nevertheless, once the long alkyl chain ligands on the surface of as-synthesized TiO_2 nanorods are removed, the TiO_2 nanorods tend to aggregate and cannot be dispersed uniformly within conducting polymer, which will hinder the photovoltaic performance. In fact, using mixed solvent to control the dispersion of nanocrystals in polymer matrix is another

* To whom correspondence should be addressed. E-mail: chunwei@ntu.edu.tw.

† These authors contributed equally to this work.

10.1021/jp1075516
Published on Web 10/08/2010

crucial factor to overcome the above issue and to achieve the relatively higher power conversion efficiency compared to other groups' reports,[4,5] but the effects have not been addressed.[6] Besides, although much effort has been devoted to developing new materials and morphology control, deeper understanding of photophysics, charge generation, and charge transport under different morphology is required for further insight into device design and optimization. Herein, we would like to demonstrate a facile method to control the nanoscale morphology of P3HT/TiO_2 nanorod hybrids by using a simple mixed solvent method. The effects of the controlled morphology on the optical and electrical properties will be discussed. More efficient carrier generation upon photoexcitation and higher carrier mobility are found in highly ordered P3HT domains. The morphology of the P3HT/TiO_2 blend controlled by using mixed solvent consists of highly crystalline nanostructured polymer domains with well-dispersed TiO_2 nanorods. The formation of an interpenetrating and percolating P3HT/TiO_2 nanorod BHJ network by using mixed solvent gives rise to efficient charge transfer and carrier transport and better photovoltaic performance. The photophysical properties, carrier transport, and carrier recombination of the polymer/TiO_2 BHJs will be investigated systematically by time-resolved photoluminescence (TRPL) spectroscopy, carrier extraction by linearly increasing voltage (CELIV) mobility measurement, and transient open-circuit voltage decay (TOCVD) measurement, respectively. This simple process does not need any further thermal post-treatment, which is compatible with the room temperature process developed with commonly used plastic substrates for flexible solar cell applications.

2. Experimental Section

2.1. Sample Preparation. P3HT ($M_W \sim 60\,000$, PDI = 1.5, RR > 96%) was first dissolved completely in chloroform (CF) (20 mg mL^{-1}) at room temperature. TiO_2 nanorods were dispersed in either CF or a *solvent mixture* consisting of pyridine, dichloromethane, and CF (1:2:2 by volume ratio) to form TiO_2 solutions (10 mg mL^{-1}). The synthesis and characterization of TiO_2 nanorods (~4−5 nm in diameter and 20−30 nm in length) were described elsewhere.[6,21] The P3HT/TiO_2 (1:1 by weight) hybrid solutions were prepared by adding 0.5 mL of P3HT solution into 1 mL of TiO_2 solution. Pristine P3HT solutions for thin-film fabrication were prepared by similar procedure. The resulting concentration of P3HT in each solution is identical (~6.7 mg mL^{-1}), and the overall ratio (by volume) of pyridine, dichloromethane, and CF in mixed solvent solutions is approximately 13:27:60. These solutions were then stirred overnight (>12 h) at room temperature before spin-coating. During the moderate stirring, the color of the mixed solvent solutions changes gradually from clear orange to dark purple. The solutions used for absorption measurement were further diluted ~100 times.

Pristine P3HT and P3HT/TiO_2 thin films for optical and atomic force microscopy (AFM) measurements were prepared by spin-coating the solutions onto cleaned glass substrates. For photovoltaic devices, P3HT/TiO_2 solutions were spin-coated onto cleaned ITO substrates covered with a precoated thin layer (~30 nm) of poly(3,4-ethylenedioxythiophene):poly(styrenesulfonic acid) (PEDOT:PSS) in nitrogen-purged glovebox. The thickness of active layers is ~200 nm. Before thermal evaporation of Al electrode in vacuum ($\sim 10^{-6}$ torr), an additional TiO_2 thin layer was spin-coated onto the active layer to act as optical spacer[22] or hole-blocking layer.[21] The samples for transmission electron microscopy (TEM) were prepared by floating the P3HT/TiO_2 thin films (on PEDOT:PSS/ITO) in deioned water and transferring the films to Cu grids.

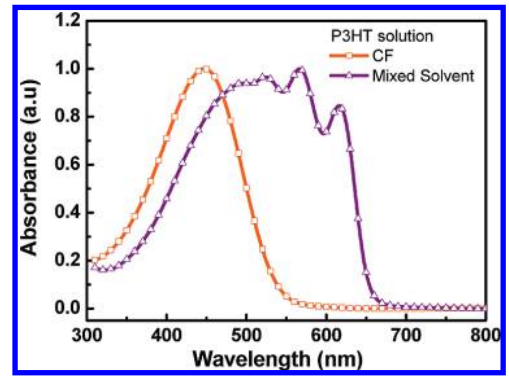

Figure 1. Absorption spectra of P3HT dilute solution (67 μg mL^{-1}) in CF and mixed solvent.

2.2. Characterizations. Solution and solid-state absorption spectra were recorded with a Jasco V570 UV/vis/NIR spectrophotometer. For TRPL measurements, a 470 nm pulsed laser (fwhm ~70 ps) operating at 20 MHz was used as excitation source and the power was kept low (0.15mW, ca. 150 pJ cm^{-2} $pulse^{-1}$). The excitation wavelength for photoluminescence (PL) measurements is also 470 nm. To avoid degradation, samples were mounted onto a cryostat under vacuum ($\sim 10^{-3}$ torr) during the measurement. PL spectra were recorded with a photomultiplier tube. TRPL spectra were recorded with a single photon avalanche photodiode connected to a time-correlated single photon counting (TCSPC) module (Picoharp300, PicoQuant) with temporal resolution 4 ps. The detection wavelength is 650 nm. Surface morphology of thin films was recorded with AFM (Nanocsope IIIA, Digital Instrument) operating in tapping mode. TEM images were recorded by FEI Tecnai 20 operating at 200 kV.

$I-V$ curves were measured using a Keithley 2410 source meter under AM 1.5 illumination (100 mW cm^{-2}) provided by solar simulator (Newport Inc.). CELIV measurements were conducted by applying a triangular voltage pulse $V(t) = At$ (reverse bias) to the devices at short-circuit conditions, and the transient curves were recorded by a digital oscilloscope (Tetronix TDS5052B). No forward bias offset was intentionally applied. For TOCVD measurements, the devices were held at V_{oc} under AM 1.5 bias light. A frequency-doubled Nd:YAG pulsed laser (532 nm, 10 Hz, pulse duration ~5 ns) was used to generate the perturbation of photovoltage. The intensity of AM 1.5 bias light was adjusted by using a series of neutral density filters. All the $I-V$ characteristics and CELIV and TOCVD measurements were performed under vacuum ($\sim 10^{-3}$ torr) in a home-built chamber.

3. Results and Discussions

3.1. Formation of Pristine P3HT Nanofibers by Mixed Solvent. Figure 1 shows the absorption spectra of dilute P3HT solutions (~67 μg mL^{-1}) in CF and mixed solvent which consists of pyridine (a poor solvent for P3HT), dichloromethane, and CF (a good solvent for P3HT). A significant red-shift and additional, well-structured vibronic features ($\lambda \sim 525$, 565, and 615 nm) were observed in the absorption spectra of the mixed solvent solution. These vibronic features are similar to those found in thin films, suggesting the formation of P3HT aggregates or nanofibers[16,23] in mixed solvent. For thin-film fabrication, solutions of higher concentrations (6.7 mg mL^{-1}) were used. The resulting morphology of pristine P3HT thin films spun from CF and mixed solvent was investigated by AFM operating in tapping mode. The surface morphology of P3HT spun from CF

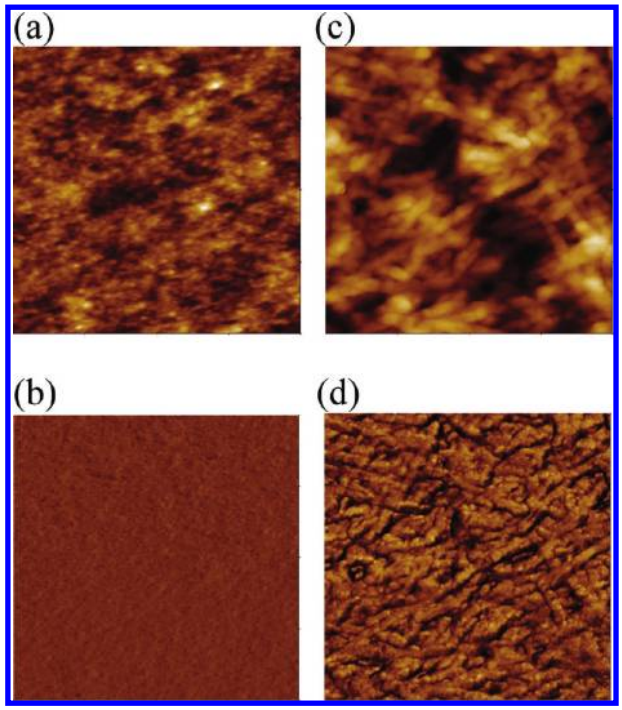

Figure 2. Tapping mode AFM images of pristine P3HT thin films spun from (a, b) CF and (c, d) mixed solvent. (a) and (c) are height images; (b) and (d) are phase images. The dimension of all images is 1 μm × 1 μm. Note that the high scale is 10 and 75 nm for (a) and (c), respectively. The phase contrast is 10° for both (b) and (d).

is very smooth with roughness (root-mean-square) about 0.78 nm (Figure 2a, b), while the morphology of the film spun from mixed solvent has distinct features consisting of a fibrous crystalline structure about several hundred nanometers in length (Figure 2c, d). A similar method to control the degree of aggregation/crystallinity of the P3HT has been reported in polymer−fullerene hybrids,[16,24] and the long axis of P3HT fibers has been assigned to the direction of π-stacking.[25,26] The low boiling point (61 °C) and high volatility of CF usually result in a fast solvent evaporation rate during the film-forming process. Kinetically limited self-organization in the as-spun film from CF thus accounts for the absence of fine structures in the absorption (Figure 3a) and PL spectra (Figure 3b), consistent with its smooth, almost featureless film morphology. In contrast, the film spun from mixed solvent shows distinct vibronic features in the absorption and PL spectra resulting from enhanced $\pi-\pi$ stacking and crystallinity of preformed P3HT aggregates. This has been further confirmed by X-ray diffraction (see the Supporting Information). In comparison, we have further performed solvent annealing process to improve the $\pi-\pi$ stacking of the P3HT film spun from CF by placing the film into a closed Petri dish with saturated CF vapor[27] for 30 min. There is an apparent enhancement in the interchain $\pi-\pi^*$ absorption (the lowest energy vibronic feature[28]) after such treatment, although it is not as intense as that in the film spun from mixed solvent.

The photophysics of P3HT thin films has been investigated by TRPL spectroscopy (Figure 3c). The PL transient curves for all samples show a monoexponential decay, while the PL lifetime (τ_{PL}) for the film spun from mixed solvent is much shorter (414 ps) compared to that for as-spun film from CF (736 ps). Such an interesting phenomenon, the negative dependence of PL lifetime on structural or interchain order, to the best of our knowledge, has not yet been well-studied. It has been reported that the PL transition in highly ordered P3HT is

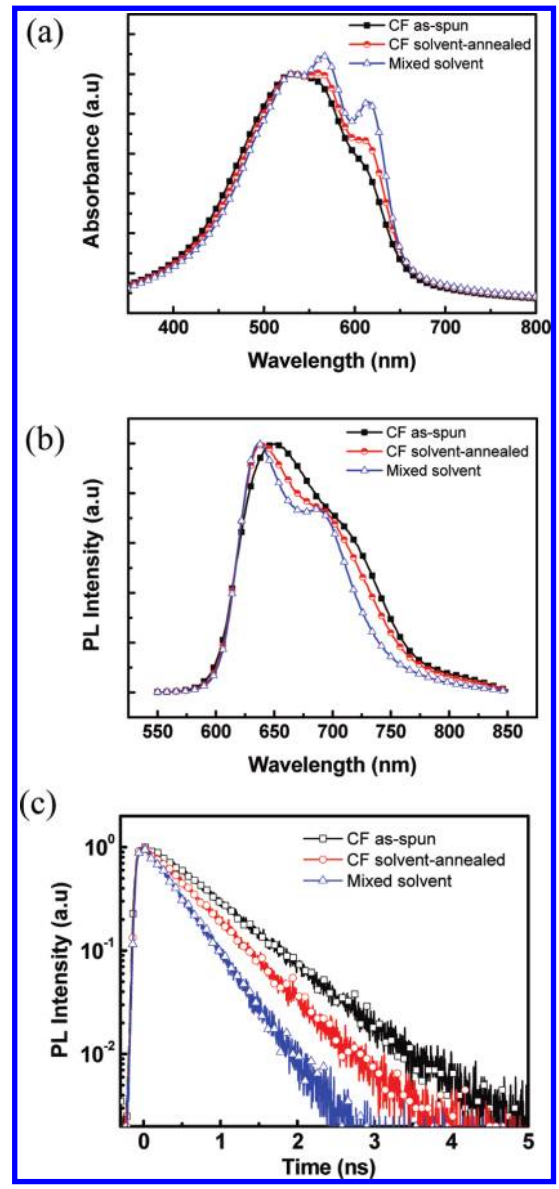

Figure 3. Optical properties of pristine P3HT thin films: (a) absorption spectra; (b) PL spectra. The absorption and PL spectra are normalized at 530 nm and emission maxima, respectively, for clarity. (c) Corresponding TRPL spectra.

optically forbidden.[29,30] Therefore, the shorter PL lifetime in higher structural order films should be attributed to nonradiative decay channels. After it is corrected to the optical density, we have also found that the PL intensity of P3HT spun from mixed solvent is only ~70% of that in P3HT spun from CF, consistent with the lower PL efficiency in the more ordered P3HT chains,[31] indicating that the nonradiative decay channel is responsible for the faster PL decay. However, there are less defects or traps in the higher structural order films that defect quenching should be suppressed. Intersystem crossing to triplet states has been shown to be absent in regioregular P3HT.[29,32] Moreover, the excitation intensity was kept low, and the measured lifetime is constant over a range of excitation intensity. High-order mechanisms such as exciton annihilation[33] can be ruled out. We thus proposed that, in highly ordered P3HT with strong interchain interaction, the emissive excitons could be separated to form interchain polaron pairs bound by Coulomb potential, leaving a positive polaron on one chain and a negative polaron on the neighboring chain.[32,34,35] These polaron pairs are likely to further dissociate into free charge carriers. It should be noted

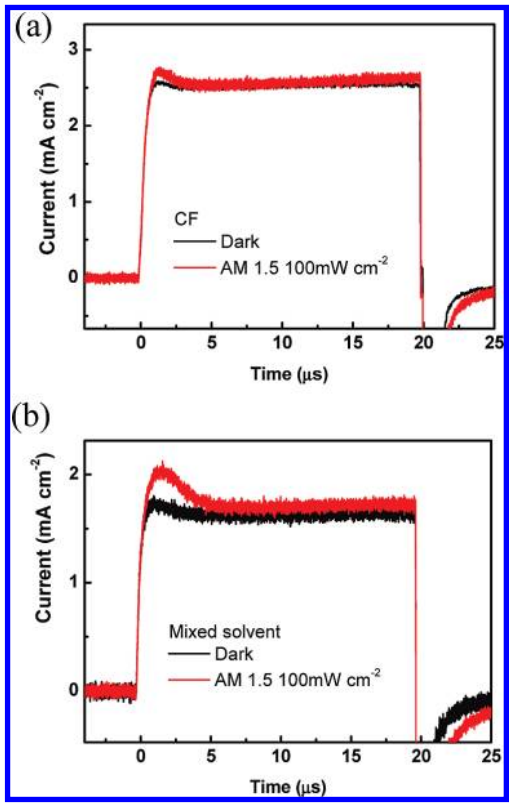

Figure 4. CELIV transient curves of pristine P3HT devices under dark and steady-state illumination. The initial step is caused by the capacitance of the film.[39,40] In order to estimate the carrier concentrations, the devices were held at short-circuit conditions without forward bias offset. Under illumination, more charge carriers are extracted in P3HT spun from mixed solvent.

that we could not distinguish whether the product of interchain charge separation process is polaron pairs or charge carriers. Direct formation of charge carriers from emissive species is also possible. For highly ordered P3HT where excitons are more delocalized among chains and the interchain interaction prevails, which causes a strong mixing of exciton state and interchain charge transfer state,[32,35] the interchain charge separation process should be more pronounced. Dissociation of emissive excitons into polaron pairs or charge carriers therefore reduces the PL (exciton) lifetime.

The charge carrier generation in conjugated polymer after photoexcitation is of great importance and has also been intensively studied by other spectroscopic techniques.[36−38] In order to further support the mechanism deduced from spectroscopic results, we have estimated the photogenerated carrier concentrations of the P3HT films by CELIV measurement.[39,40] The device structure is Al/P3HT/PEDOT:PSS/indium tin oxide (ITO), similar to the structure of photovoltaic devices. In the CELIV measurement, both the carrier mobility and concentration can be estimated simultaneously. The carrier mobility μ of pristine P3HT thin films can be calculated according to[39]

$$\mu = \frac{2d^2}{3At_{max}^2}$$

where d is the thickness of the sample, A is the voltage ramp rate, and t_{max} is the time the extraction current reaches maximum. Figure 4 shows the transient curves of pristine P3HT devices under dark and AM 1.5 illumination. P3HT spun from mixed solvent shows a higher carrier mobility (5.4×10^{-4} cm^2 V^{-1} s^{-1}) when compared to the film spun from CF (2.6×10^{-4} cm^2 V^{-1} s^{-1}). The conductivity σ, which can also be estimated from the transient curves,[40] allows us to obtain the carrier concentration n according to $\sigma = ne\mu$. In the dark condition, the charge carrier concentrations of the film spun from CF (1.1×10^{14} cm^{-3}) and mixed solvent (1.2×10^{14} cm^{-3}) are very close. While the samples are under AM 1.5 illumination (100 mW cm^{-2}), the charge carrier concentration in the film spun from mixed solvent (5.9×10^{14} cm^{-3}) is about 2 times higher than that in the film spun from CF (2.8×10^{14} cm^{-3}), indicating more dissociated free carriers exist in the nanostructured P3HT. From the above results of TRPL and CELIV measurement, we conclude that the charge carrier generation is more efficient in highly ordered P3HT domains spun from mixed solvent.

3.2. Morphology Control of P3HT/TiO_2 BHJs by Mixed Solvent. Next, we have examined the controlled nanoscale morphology of P3HT/TiO_2 nanorod hybrids and the correlation to the optical and electrical properties. The hybrid films were fabricated by blending TiO_2 nanorods into P3HT (1:1 by weight) to form BHJs. The surface of as-synthesized TiO_2 nanorods was capped with surfactants, oleic acid (O.A.), which contain long alkyl chains acting as a barrier for charge transport and charge transfer.[12] In order to improve the device performance, the surfactants on TiO_2 nanorod surface have been removed by pyridine treatment.[6,12] These nanorods were then vacuum-dried to form powder before redispersion in CF or solvent mixture. However, after removal of surfactants on the TiO_2 surface, the nanorods tend to form small agglomerates in CF, whereas they can be easily dispersed in pyridine (see the Supporting Information). Figure 5a, b shows the tapping-mode AFM images of the hybrid film spun from CF. The islands as shown in the height image (Figure 5a) appear as clusters of bright spots in the corresponding phase image (Figure 5b). Since the phase-shift reflects the relative materials hardness, these clusters showing different contrast from the matrix are attributed to be small agglomerates of TiO_2 nanorods.[41] Figure 5d, e shows the surface morphology of P3HT/TiO_2 film spun from mixed solvent where TiO_2 nanorods are found to be more homogeneously dispersed in the film. This result can be further supported from the TEM images (Figure 5c, f), which reveal the bulk properties of the thin films. The TEM image for the films spun from CF shows that TiO_2 nanorods have clearly aggregated into domains in contrast to a relatively uniform dispersion in the hybrid film after using mixed solvent. In the mixed solvent solution, the presence of pyridine can not only induce P3HT aggregates but also facilitate the dispersion of nanorods in the hybrid solution. During the film-forming process by mixed solvent, the P3HT aggregates to form a nanostructured network and the TiO_2 nanorods, which can be dispersed in pyridine, subsequently infiltrate to fill the space between these P3HT nanostructures. This leads to a morphology with well-distributed TiO_2 nanorods embedded in highly crystalline polymer domains to form a bicontinuous phase separation which may be beneficial for both charge transfer and charge transport in BHJ solar cells.

Figure 6a shows the absorption of P3HT/TiO_2 films spun from CF and mixed solvent. The absorption of P3HT/TiO_2 hybrid films is simply the superposition of the two components without any apparent shift. The vibronic features in the hybrid film spun from mixed solvent are still clearly resolved, indicating that the characteristic of ordered P3HT nanostructure is nearly preserved after adding TiO_2 nanorods, although the intensity of this vibronic peak is slightly weaker than pristine P3HT spun from mixed solvent. The PL and TRPL spectra of the P3HT/TiO_2

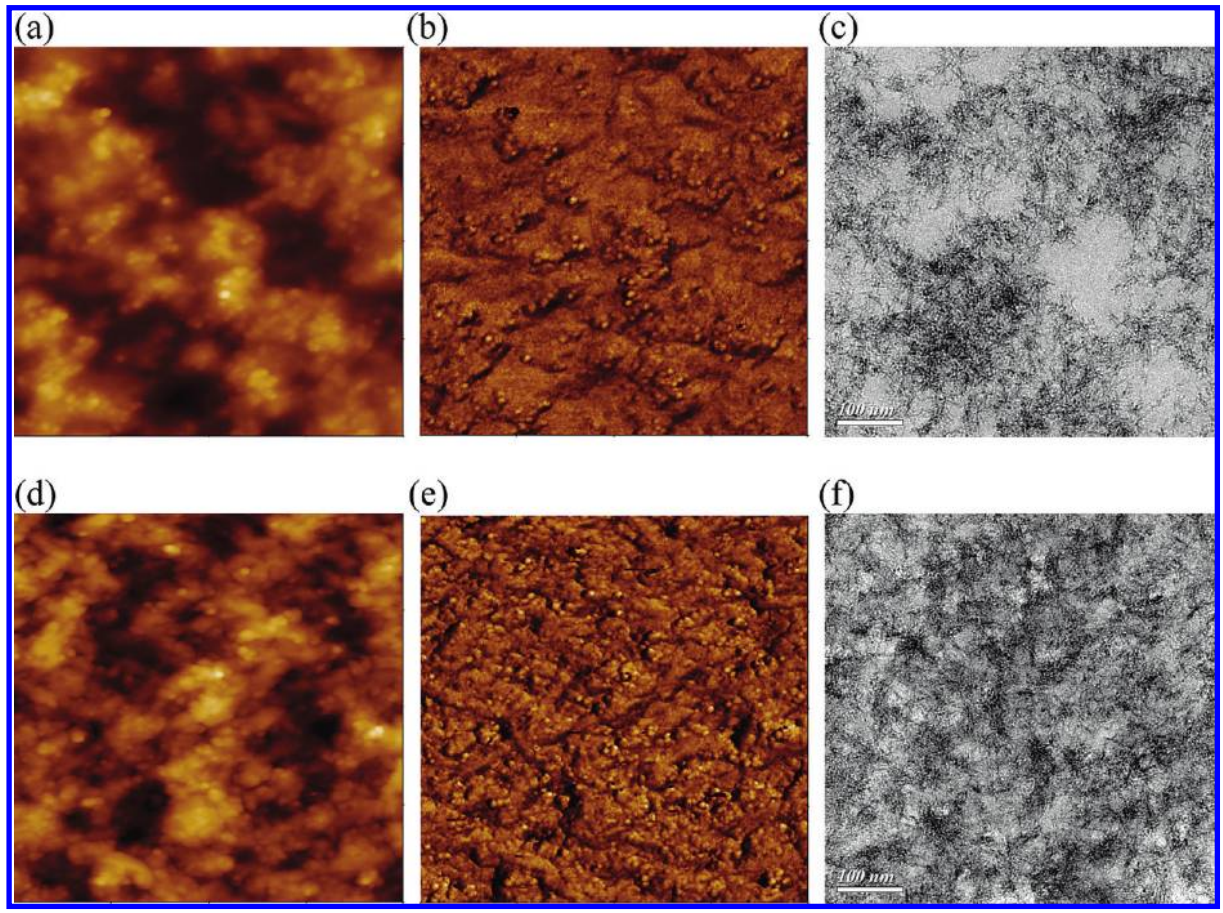

Figure 5. Morphology of P3HT/TiO_2 hybrid films spun from CF (a−c), and mixed solvent (d−f). (a) and (d) are AFM height images. The height scale is 75 nm. (b) and (e) are AFM phase images. The phase contrast is 10°. The dimension of all AFM images is 1 μm × 1 μm. (c) and (f) are TEM images.

hybrid films are shown in Figure 6b and 6c, respectively. The PL spectral shapes of P3HT/TiO_2 hybrid films are similar to those of pristine P3HT thin films spun from the same solvent, but the corresponding PL intensities are significantly quenched, due to another efficient nonradiative channel for charge transfer from P3HT to TiO_2. The PL quenching efficiency is 78% and 87% for hybrid films spun from CF and mixed solvent, respectively (compared to pristine P3HT spun from the same solvent). Since the pristine P3HT thin film spun from mixed solvent has a much lower PL efficiency, the difference of PL efficiency in P3HT/TiO_2 hybrid films spun from different solvents would be even larger. The enhanced charge separation efficiencies in the hybrid films can be further revealed from the PL dynamics. Figure 6c shows the transient PL decay curves of the pristine P3HT and P3HT/TiO_2 hybrid thin films spun from different solvents. The addition of TiO_2 nanorods in P3HT creates a large number of interfaces for charge separation, resulting in shortening of PL lifetime and quenching of PL intensities. The measured PL lifetime can be expressed as

$$\frac{1}{\tau_{\text{hybrid}}} = \frac{1}{\tau_{\text{R}}} + k_{\text{P3HT}} + k_{\text{TiO}_2}$$

where τ_{hybrid} is the measured PL lifetime in P3HT/TiO_2 hybrid films and τ_{R} is the natural radiative recombination lifetime of pristine P3HT; k_{P3HT} is the nonradiative rate resulting from dissociated excitons and other intrinsic nonradiative mechanisms within P3HT; and k_{TiO_2} is the nonradiative rate from charge transfer process at P3HT/TiO_2 interfaces. For the P3HT/TiO_2 hybrid film spun from mixed solvent, much shorter τ_{hybrid} was observed. This is attributed to both the enhanced k_{P3HT} resulting from highly ordered P3HT domains and enhanced k_{TiO_2} resulting from well-dispersed TiO_2 nanorods, giving rise to an overall enhanced charge separation efficiency with a higher PL quenching efficiency and charge transfer rate.

3.3. Device Performance. Figure 7 shows the current−voltage characteristics of the photovoltaic devices using P3HT/TiO_2 nanorod hybrid films as an active layer, which were prepared using the same procedures as discussed above. The devices structure is ITO/PEDOT:PSS/P3HT:TiO_2/TiO_2/Al with an additional TiO_2 thin layer acting as an optical spacer[22] or hole-blocking layer.[21] The device spun from CF shows a short-circuit current (J_{sc}) of 1.31 mA cm^{-2}, an open circuit voltage (V_{oc}) of 0.49 V, and a fill factor (FF) of 0.50 under simulated AM 1.5 illumination (100 mW cm^{-2}), giving a power conversion efficiency of 0.32%. A significant improvement of the photovoltaic performance is achieved in the device consisting of the hybrid film spun from mixed solvent, giving an increased J_{sc} (2.78 mA cm^{-2}), V_{oc} (0.65 V), and FF (0.56) and a power conversion efficiency of 1.01%. The enhancement of the J_{sc} could be attributed to the increased charge separation efficiency for the sample deposited by using mixed solvent which consists of well-dispersed TiO_2 nanorods within nanostructured P3HT matrix. We believe that interchain charge separation process discussed previously also contributes to the improved J_{sc} because more charge carriers can be generated in highly ordered P3HT domains. Nevertheless, the charge carrier generation efficiency alone might not be sufficient to explain the twofold improvement

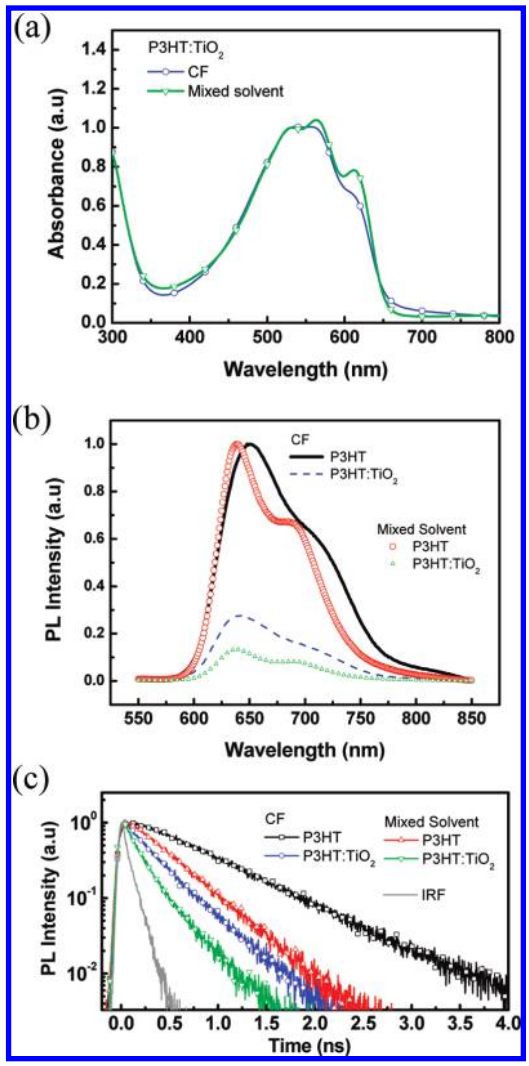

Figure 6. Optical properties of P3HT/TiO_2 hybrid thin films: (a) normalized (at 530 nm) absorption spectra of thin films spun from CF and mixed solvent; (b) PL spectra. The relative intensity of hybrid films to pristine P3HT has been corrected to the fraction of photons absorbed; the intensity of pristine P3HT thin films was scaled to unity for comparison. (c) Corresponding TRPL spectra. Also shown is the instrument response function (IRF).

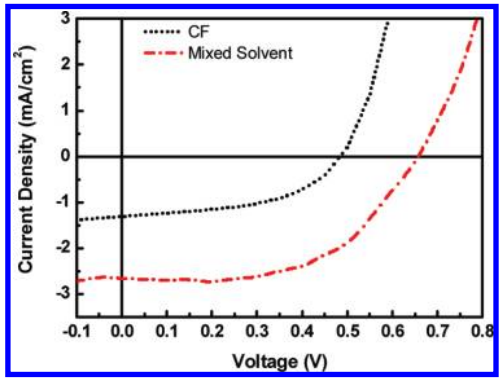

Figure 7. Current−voltage characteristics of P3HT/TiO_2 photovoltaic devices spun from CF and mixed solvent. The measurements were performed under simulated AM 1.5 illumination (100 mW cm^{-2}).

of J_{sc} as PL quenching efficiencies in both devices are greater than 50%. The improvement, therefore, may also originate from enhanced charge collection efficiency. Once the photogenerated electron−hole pairs are separated at interfaces, they will either be transported toward the collecting electrodes to generate

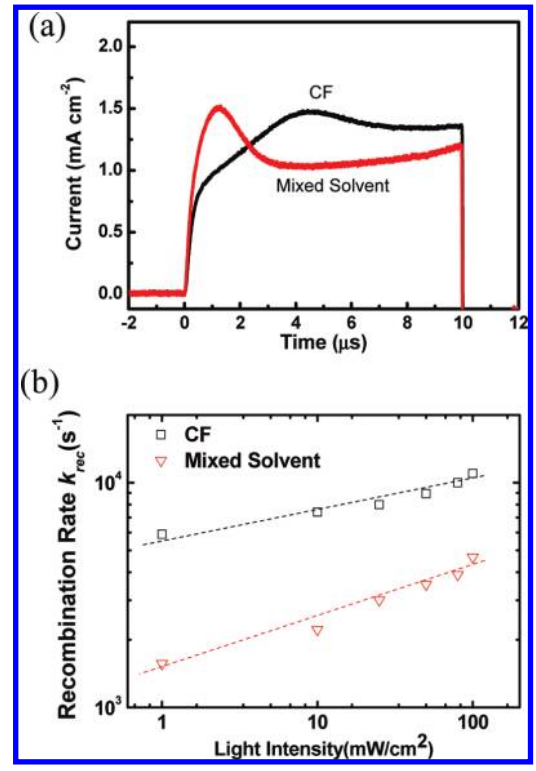

Figure 8. Electrical properties of P3HT/TiO_2 photovoltaic devices. (a) CELIV transient curves of P3HT/TiO_2 photovoltaic devices (measured under dark conditions). (b) Charge carrier recombination rate constants determined by TOCVD measurements at different illumination levels. The straight lines are guides to the eye.

current or recombine again to lose their energy. Thus, we have further performed CELIV and TOCVD measurements to estimate the carrier mobilities and recombination rates of these operating devices. Compared to the conventional methods such as the space-charge limited current (SCLC) technique, in which a change of electrodes materials is required, or the time-of-flight (TOF) method, in which a much thicker film is required, the CELIV technique provides a direct measurement of carrier mobility on the actual photovoltaic devices without changing the electrodes or film morphology. As determined from the transient curves shown in Figure 8a, the carrier mobility of the device spun from mixed solvent is 7.7×10^{-4} cm^2 V^{-1} s^{-1}, about an order higher than that of 6.2×10^{-5} cm^2 V^{-1} s^{-1} for the device spun from CF. The CELIV generally measures the mobility of majority carriers,[39] which are holes in the P3HT/TiO_2 hybrid solar cells. For the device spun from mixed solvent, the higher crystallinity of P3HT domains can facilitate hole transport, leading to the improvement of measured carrier mobility. In addition, it has been suggested by Tuladhar et al. that blending electron acceptors into polymers could change the hole mobility,[42] and the connectivity of nanocrystals in polymer matrix could be a limiting factor for charge collection.[11] The distribution of TiO_2 in P3HT matrix should also be considered. For the device spun from CF, the presence of small TiO_2 agglomerates can also block the transport pathways and thus impede hole transport in P3HT. In the operation of photovoltaic devices, such morphology might also be unfavorable for electron transport through TiO_2 since more hopping steps are required. This probably explains the lower mobility value of the device spun from CF when compared to that of the pristine P3HT film (1.6×10^{-4} cm^2 V^{-1} s^{-1}). In contrast, the bicontinuous phase-separated morphology in the device spun from mixed solvent can provide more effective transport pathways for both electrons

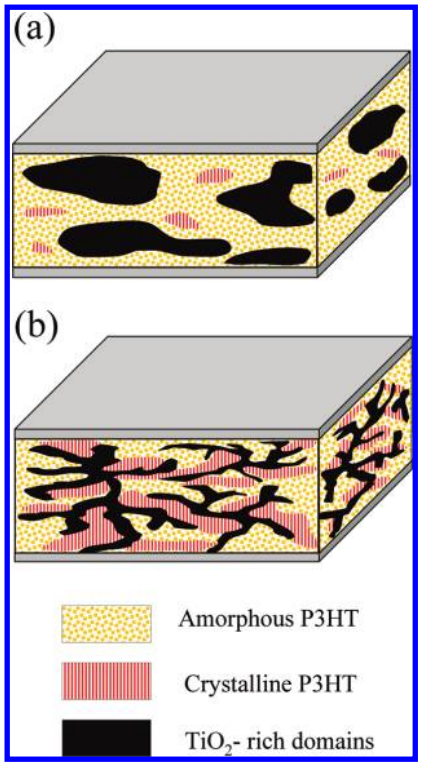

Figure 9. Schematic representations of the nanoscale morphology of P3HT/TiO_2 thin films spun from (a) CF and (b) mixed solvent. Matrix, amorphous P3HT; red line pattern, crystalline P3HT; black region, TiO_2-rich domain. (Not drawn to scale.)

and holes. The photogenerated carriers are more likely successfully transported to the electrodes and collected as photocurrent. The enhanced performance of the device with morphology controlled by mixed solvent can be further supported from the reduced recombination rates investigated by the TOCVD measurement. During the measurements, the devices were illuminated at a bias white light and were then operated at a steady-state condition of V_{oc}. A small perturbation by a pulsed laser is used to generate extra electrons and holes. The decay of the photovoltage generated by the additional carriers due to small perturbation corresponds to the recombination rate at heterojunctions. Figure 8b plots the charge recombination rate constant k_{rec} versus illumination intensity for the two devices under an open-circuit condition. It was found that the recombination rates k_{rec} at all light intensities are lower for the device using mixed solvent compared to that using CF. Suppression of back recombination at interfaces leads to an increased number of carriers which can be transported toward electrodes, contributing to the improved J_{sc}. In addition, the reduced recombination rate at interfaces will also increase the difference between the quasi-Fermi levels of electrons and holes of devices,[6] giving a higher value of V_{oc}. Consequently, the morphology controlled by using mixed solvent is crucial to improve photovoltaic performance of P3HT/TiO_2 BHJ solar cells. The schematic representations of the nanoscale morphology of P3HT/TiO_2 nanorod hybrid thin films spun from CF and mixed solvent are shown in Figure 9. The preformed P3HT nanostructured domains for films spun from mixed solvent can facilitate the dispersion of TiO_2 nanorods, giving a bicontinuous phase-separated morphology with an increased number of interfaces and more effective carrier transport pathways to improve charge separation, transport, and recombination in P3HT/TiO_2 nanorod BHJs.

4. Conclusions

In conclusion, we have presented a simple approach by using mixed solvent to control the morphology of P3HT/TiO_2 nanorod hybrid BHJs without any post-treatment. The use of mixed solvent not only results in highly crystalline P3HT domains but also assists the dispersion of TiO_2 nanorods within polymer matrix. The highly crystalline P3HT domains can show higher carrier generation efficiency upon photoexcitation. The formation of a bicontinuous phase-separated morphology for the hybrid film by using mixed solvent can largely enhance charge separation and transport efficiencies which are crucial for efficient polymer/inorganic nanocrystal hybrid solar cells. Our method for morphology control could also be applied to other donor−acceptor blends as a strategy for device optimization, especially to those incompatible in single solvent. The lower efficiency than the most studied polymer:fullerene composites may come from intrinsic properties of materials such as surface defects and traps in nanocrystals[4] or slower charge transfer rate between polymers and inorganic nanocrystals. Therefore, further improvements can be expected by improving the crystalline quality, surface modification of nanocrystals,[6] or tuning the dimensions of nanocrystals.

Acknowledgment. This work is supported by the National Science Council, Taiwan (Project No. NSC 96-2112-M-002-030-MY3 and 95-3114-P-002-003-MY3).

Supporting Information Available: X-ray diffraction, dispersion of TiO_2 in solvents, and photographs of solution for thin-film fabrication. This material is available free of charge via the Internet at http://pubs.acs.org.

References and Notes

(1) Yu, G.; Gao, J.; Hummelen, J. C.; Wudl, F.; Heeger, A. J. *Science* **1995**, *270*, 1789.
(2) Chen, L.-M.; Hong, Z.; Li, G.; Yang, Y. *Adv. Mater.* **2009**, *21*, 1434.
(3) Park, S. H.; Roy, A.; Beaupre, S.; Cho, S.; Coates, N.; Moon, J. S.; Moses, D.; Leclerc, M.; Lee, K.; Heeger, A. J. *Nat. Photonics* **2009**, *3*, 297.
(4) Boucle, J.; Chyla, S.; Shaffer, M. S. P.; Durrant, J. R.; Bradley, D. D. C.; Nelson, J. *Adv. Funct. Mater.* **2008**, *18*, 622.
(5) Kwong, C. Y.; Djurisic, A. B.; Chui, P. C.; Cheng, K. W.; Chan, W. K. *Chem. Phys. Lett.* **2004**, *384*, 372.
(6) Lin, Y. Y.; Chu, T. H.; Li, S. S.; Chuang, C. H.; Chang, C. H.; Su, W. F.; Chang, C. P.; Chu, M. W.; Chen, C. W. *J. Am. Chem. Soc.* **2009**, *131*, 3644.
(7) Huynh, W. U.; Dittmer, J. J.; Alivisatos, A. P. *Science* **2002**, *295*, 2425.
(8) Huynh, W. U.; Dittmer, J. J.; Libby, W. C.; Whiting, G. L.; Alivisatos, A. P. *Adv. Funct. Mater.* **2003**, 73.
(9) McDonald, S. A.; Konstantatos, G.; Zhang, S.; Cyr, P. W.; Klem, E. J. D.; Levina, L.; Sargent, E. H. *Nat. Mater.* **2005**, *4*, 138.
(10) Beek, W. J. E.; Wienk, M. M.; Janssen, R. A. J. *Adv. Funct. Mater.* **2006**, *16*, 1112.
(11) Oosterhout, S. D.; Wienk, M. M.; van Bavel, S. S.; Thiedmann, R.; Koster, L. J. A.; Gilot, J.; Loos, J.; Schmidt, V.; Janssen, R. A. J. *Nat. Mater.* **2009**, *8*, 818.
(12) Lin, Y. Y.; Chu, T. H.; Chen, C. W.; Su, W. F. *Appl. Phys. Lett.* **2008**, *92*, 053312.
(13) Ma, W.; Yang, C.; Gong, X.; Lee, K.; Heeger, A. J. *Adv. Funct. Mater.* **2005**, *15*, 1617.
(14) Li, G.; Yao, Y.; Yang, H.; Shrotriya, V.; Yang, G.; Yang, Y. *Adv. Funct. Mater.* **2007**, *17*, 1636.
(15) Park, Y. D.; Lee, H. S.; Choi, Y. J.; Kwak, D.; Cho, J. H.; Lee, S.; Cho, K. *Adv. Funct. Mater.* **2009**, *19*, 1200.
(16) Berson, S.; Bettignies, R. D.; Bailly, S.; Guillerez, S. *Adv. Funct. Mater.* **2007**, *17*, 1377.
(17) Peet, J.; Kim, J. Y.; Coates, N. E.; Ma, W. L.; Moses, D.; Heeger, A. J.; Bazan, G. C. *Nat. Mater.* **2007**, *6*, 497.
(18) Lee, J. K.; Ma, W. L.; Brabec, C. J.; Yuen, J.; Moon, J. S.; Kim, J. Y.; Lee, K.; Bazan, G. C.; Heeger, A. J. *J. Am. Chem. Soc.* **2008**, *130*, 3619.

(19) Campbell, A. R.; Hodgkiss, J. M.; Westenhoff, S.; Howard, I. A.; Marsh, R. A.; McNeill, C. R.; Friend, R. H.; Greenham, N. C. *Nano Lett.* **2008**, *8*, 3942.
(20) Li, L.; Lu, G.; Yang, X. *J. Mater. Chem.* **2008**, *18*, 1984.
(21) Zeng, T. W.; Lin, Y. Y.; Lo, H. H.; Chen, C. W.; Chen, C. H.; Liu, S. C.; Huang, H. Y.; Su, W. F. *Nanotechnology* **2006**, *17*, 5387.
(22) Kim, J. Y.; Kim, S. H.; Lee, H. H.; Lee, K.; Ma, W.; Gong, X.; Heeger, A. J. *Adv. Mater.* **2006**, *18*, 572.
(23) Mehta, A.; Kumar, P.; Dadmun, M. D.; Zheng, J.; Dickson, R. M.; Thundat, T.; Sumpter, B. G.; Barnes, M. D. *Nano Lett.* **2003**, *3*, 603.
(24) Moule, A. J.; Meerholz, K. *Adv. Mater.* **2008**, *20*, 240.
(25) Aasmundtveit, K. E.; Samuelsen, E. J.; Guldstein, M.; Steinsland, C.; Flornes, O.; Fagermo, C.; Seeberg, T. M.; Pettersson, L. A. A.; Inganas, O.; Feidenhans'l, R.; Ferrer, S. *Macromolecules* **2000**, *33*, 3120.
(26) Kline, R. J.; McGehee, M. D.; Kadnikova, E. N.; Liu, J.; Frechet, J. M. J.; Toney, M. F. *Macromolecules* **2005**, *38*, 3312.
(27) Miller, S.; Fanchini, G.; Lin, Y. Y.; Li, C.; Chen, C. W.; Su, W. F.; Chhowalla, M. *J. Mater. Chem.* **2008**, *18*, 306.
(28) Brown, P. J.; Thomas, D. S.; Kohler, A.; Wilson, J. S.; Kim, J. S.; Ramsdale, C. M.; Sirringhaus, H.; Friend, R. H. *Phys. Rev. B* **2003**, *67*, 064203.
(29) Jiang, X. M.; Osterbacka, R.; Korovyanko, O.; An, C. P.; Horovitz, B.; Janssen, R. A. J.; Vardeny, Z. V. *Adv. Funct. Mater.* **2002**, *12*, 587.
(30) Clark, J.; Silva, C.; Friend, R. H.; Spano, F. C. *Phys. Rev. Lett.* **2007**, *98*, 206406.
(31) McNeill, C. R.; Halls, J. J. M.; Wilson, R.; Whiting, G. L.; Berkebile, S.; Ramsey, M. G.; Friend, R. H.; Greenham, N. C. *Adv. Funct. Mater.* **2008**, *18*, 2309.
(32) Guo, J.; Ohkita, H.; Benten, H.; Ito, S. *J. Am. Chem. Soc.* **2009**, *131*, 16869.
(33) Shaw, P. E.; Ruseckas, A.; Samuel, I. D. W. *Adv. Mater.* **2008**, *20*, 3516.
(34) Wang, Z.; Mazumdar, S.; Shukla, A. *Phys. Rev. B* **2008**, *78*, 235109.
(35) Scholes, G. D. *ACS Nano* **2008**, *2*, 523.
(36) Cook, S.; Katoh, R.; Furube, A. *J. Phys. Chem. C* **2009**, *113*, 2547.
(37) Hwang, I.-W.; Moses, D.; Heefer, A. J. *J. Phys. Chem. C* **2008**, *112*, 4350.
(38) Piris, J.; Dykstra, K. E.; Bakulin, A. A.; van Loosdrecht, P. H. M.; Knulst, W.; Trinh, M. T.; Schins, J. M.; Siebbeles, L. D. A. *J. Phys. Chem. C* **2009**, *113*, 14500.
(39) Juska, G.; Arlauskas, K.; Viliunas, M.; Kocka, J. *Phys. Rev. Lett.* **2000**, *84*, 4946.
(40) Juska, G.; Arlauskas, K.; Viliunas, M.; Genevicius, K.; Osterbacka, R.; Stubb, H. *Phys. Rev. B* **2000**, *62*, R16235.
(41) Beek, W. J. E.; Wienk, M. M.; Kemerink, M.; Yang, X.; Janssen, R. A. J. *J. Phys. Chem. B* **2005**, *109*, 9505.
(42) Tuladhar, S. M.; Poplavskyy, D.; Choulis, S. A.; Durrant, J. R.; Bradley, D. D. C.; Nelson, J. *Adv. Funct. Mater.* **2005**, *15*, 1171.

JP1075516